**ORIGINAL ARTICLE**

# Influence of Interlayer Material on Softening and Wear Behavior of Friction Stir Welded AA6061-T6 alloy

Korra Nagu[1] · MVNV Satyanarayana[2] ·
K. Harikrishna[3] · Adepu Kumar[3]

**Abstract** In this investigation, Zn and brass interlayers were used for friction stir welding (FSW) of AA6061-T6 and investigated the weld joint's microstructure, mechanical, and wear behavior. From microstructural analysis, it was observed that Zn dissolved in Al matrix at FSW process temperature and formed a solid solution. Brass particles distributed uniformly throughout the stir zone (SZ) formed a composite-like structure and intermetallic compounds (IMCs) such as $Al_2Cu$ and $Al_4Cu_9$. The grain size obtained for weld without interlayer, with Zn and brass interlayer, was 5.6 μm, 3.6 μm, and 2.3 μm, respectively. Hardness in SZ improved with brass interlayer. Marginal strength was enhanced for weld with Zn interlayer, and better strength was obtained with brass interlayer due to reduced softening and formation of IMCs than for weld without interlayer. The surface hardening mechanism reduced the wear rate for weld with brass interlayer.

**Keywords** Welding · Mechanical properties · Microstructure · Brass interlayer · Zn interlayer · Intermetallic compounds

✉ Korra Nagu
nagu.k@bvrit.ac.in

1 Mechanical Engineering Department, B. V. Raju Institute of Technology, Narsapur, Telangana 502313, India

2 Department of Mechanical Engineering, Anil Neerkonda Institute of Technology and Science, Visakhapatnam, Andhra Pradesh 531162, India

3 Department of Mechanical Engineering, National Institute of Technology, Warangal, Telangana 506004, India

## 1 Introduction

Aluminum and its alloys are widely used in various industrial applications due to their high strength-to-weight ratio [1]. Solid-state welding process, such as friction stir welding (FSW), is commonly used to join Al alloys [2]. Due to weld being carried out below the melting point of weld metal, defects such as porosity and solidification cracks can be reduced, and recrystallized fine grains can be obtained in SZ [3]. Although FSW produces fine, dynamically recrystallized grains, softening at SZ occurs due to weld thermal cycle causing a reduction in weld strength [4]. Precipitation-hardened alloys, such as AA6061, are prone to softening due to precipitate coarsening. Various researchers attempted to reduce thermal softening with water cooling and post-processing [5, 6]. Post-processing methods such as heat treatment are time-consuming and impossible to perform on non-heat-treated Al alloys. Water cooling requires an extra setup to perform welding, which is a cost-effective method. One approach to reduce thermal softening and enhance weld strength is to insert an appropriate interlayer amid weld plates to be joined. Some researchers have attempted to use interlayers to improve the mechanical properties of welds. Khojastehnezhad et al. [7] studied the effect of pure Cu insertion on the mechanical properties of FSWed AA6061. They found that Cu particles were distributed throughout the SZ, forming composite-like structures and strengthening IMCs such as $Al_2Cu$ and $Al_4Cu_9$. They concluded that strength and hardness were improved for weld with the insertion of Cu than without insert. Mokabberi et al. [8] used interlayer materials such as Zn, Cu, and brass to overcome the thermal softening of FSWed AA1050 alloy. They found that marginal improvement in mechanical properties was observed with the Zn interlayer and more enhanced with brass interlayer due to the uniform dispersion in Al matrix

and formation of IMCs. They concluded that IMCs are the key factors that decide mechanical properties' improvement. Wilson et al. [9] investigated the effect of different thicknesses of interlayers on enhancing the mechanical properties of Al7020 alloy. They concluded that the minimum average grain size obtained with a 10 μm Zn interlayer resulted in improved mechanical properties due to proper dispersion of Zn particles. Weld joint endurance is often determined by wear resistance. It is feasible to improve weld wear resistance by adding reinforcement particles. Alishavandi et al. [10] investigated a 6 pass FSP on corrosion and wear behavior with and without mischmetal oxide nanocomposite. They concluded that adding reinforcement particles acting as lubricants decreased the coefficient of friction, thereby reducing wear rate.

The existing literature has shown that interlayer insertion resulted in more grain refinement and improved mechanical properties. There is no literature on using soft and hard interlayer material on FSW of AA6061 alloy to reduce softening and improve mechanical properties. The soft material dissolves in Al matrix, and the hard material will not react with Al matrix appropriately at FSW process temperature. Hence, the present investigation focused on the effect of soft (Zn) and hard (brass) interlayers on mechanical, wear properties, and microstructure of FSWed AA6061 (Table 1).

## 2 Materials and Experimental Procedure

The base metal (BM) used in this study was a 6 mm thick AA6061 in T6 temper condition. Pure Zn and brass (58% Cu and 36% Zn) interlayers of 0.2 mm thickness were kept between the adjoining ends of weld plates, as shown in Fig. 1c. A tool consists of a cylindrical threaded pin profile made of H13 steel and entails 18 mm shoulder, 6 mm pin diameter, and 5.7 mm pin length, as shown in Fig. 1b. A 30 KN capacity FSW machine was used for welding the plates along the rolling direction. FSW experiment is represented in Fig. 1a. The process parameters used in this investigation were plunge depth, tool rotational speed and transverse speed of 0.2 mm, 800 rpm, and 25 mm/min, respectively. The samples were cut normal to the weld path and polished as per standard microstructural analysis procedure. Microstructural observations were made using electron backscatter diffraction (EBSD), scanning electron microscope (SEM), and optical microscope (OM). Microhardness measurement was performed transversely to the weld direction with 0.5 g load and 0.5 mm between successive indentations. The tensile specimen was prepared as per ASTM-E8 standard, and test was carried out using a universal testing machine with 100 KN capacity. After the tensile test, all the samples' fracture surface was studied under SEM. A dry sliding pin-on-disk wear test was performed using a TRM 500 pin on the disc machine with a tribometer. An ASTM standard G99-04 was used to conduct wear test. The corresponding discs were produced of GCr15, which had a hardness of about 50 HRC and a 0.3 mm surface roughness (Ra). According to conventional metallographic procedure, the pins were polished using grit SiC papers. Before and after the test, samples are weighed to determine the wear rate. The dry sliding wear test was conducted over 1000 m with a constant load of 30 N and a sliding velocity of 0.2 m/s.

**Table 1** Chemical composition of AA6061-T6

| Mg | Si | Cr | Mn | Fe | Cu | Ti | Zn | Al |
|------|------|------|------|------|------|------|------|-----|
| 0.79 | 0.83 | 0.06 | 0.04 | 0.21 | 0.22 | 0.03 | 0.02 | Bal |

**Fig. 1** **a** FSW experiment, **b** Tool used for welding, and **c** FSW schematic with interlayer
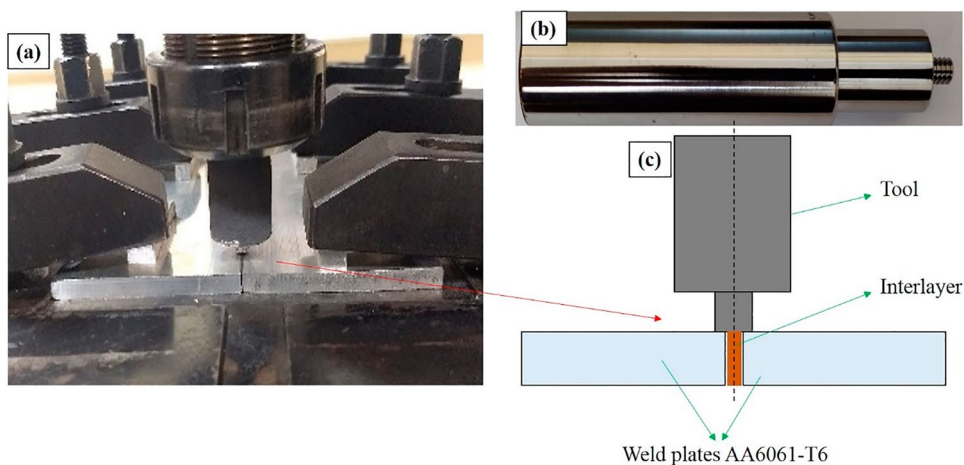
## 3 Results and Discussion

The macrostructure of weld with different conditions is displayed in Fig. 2. Defect-free weld was obtained without and with interlayer attributed to sufficient heat generated at optimum parameters. Weld without interlayer shows a typical onion ring structure (Fig. 2a), confirming proper material flow. Furthermore, the mixing of Zn in SZ was observed for welding with Zn interlayer (Fig. 2b), and forming a composite-like structure. Fine grain structure was observed for weld without interlayer (Fig. 3a). Uniform distribution of Zn in SZ for weld with Zn interlayer was observed (Fig. 3b). The distribution of small brass particles was observed for weld with a brass interlayer (Fig. 3c). This was due to the tool rotational speed, which fractured Zn and brass, and led to scattering in SZ. Welds with the distribution of Zn and brass formed composite-like structures (Fig. 2b and c). More particle accumulation (Zn and brass) was identified on

the advancing side (AS). Generally, material flow from the retreating side (RS) to AS and temperature generated on AS was higher during FSW. Basin-shaped SZ (Fig. 2a and 2b) was observed for welding without and with Zn interlayer. Furthermore, elliptical-shaped SZ was observed for weld with brass interlayer. The SZ shape is mainly governed by interlayer material, weld material, tool geometry, reinforcements, thermal conductivity, base metal temperature, and process parameters [11].

The intermetallic and precipitate behavior were studied with the help of SEM analysis and represented in Fig. 4. During FSW, small precipitates were distributed uniformly in SZ for weld without interlayer, as shown in Fig. 4a. Furthermore, due to high diffusion rate of Zn in Al matrix, Zn particles may dissolve and be disseminated in the Al matrix. As a result, the Zn interlayer in the weld first fractured into tiny pieces before dissolving and dispersing to produce an Al-Zn solid solution (Fig. 4b). Generally, Zn possesses high thermal conductivity and low melting point. During FSW, the temperature exceeds Zn's melting point, which leads to dissolution and diffuses in the Al matrix [8]. The diffusion of brass particles in the Al matrix (Fig. 4c) could be attributed to the possibility of an interdiffusion reaction between Al and brass. A thin layer of diffusion occurred at the interface because the weld was subjected to adequate heat under optimum parameter conditions. IMCs formation is feasible at interfaces when diffusion is permitted, and Al and Cu are simultaneously present in a system. In addition, solid-state diffusion between the Al matrix and the brass particle in SZ can produce IMCs [12]. During FSW, brittle IMCs developed, resulting in a few voids and cracks along the interface (Fig. 4c). EDAX line scan was carried out on the weld with brass interlayer, as indicated in Fig. 5a and b, to check the interaction and diffusion of brass particles in Al matrix. A line was chosen for EDAX scan in the cross sectional SEM image (Fig. 5a), and the resulting elemental intensity curves are depicted in Fig. 5b. The width of the curve's interface (Fig. 5b) suggests that the reaction between brass particles and Al matrix is relatively comprehensive.
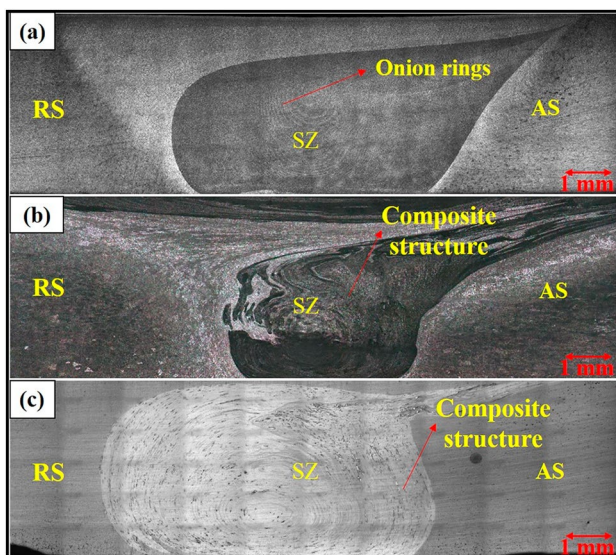


**Fig. 2** Macrostructure of welds **a** without interlayer, **b** with Zn interlayer, and **c** with brass interlayer
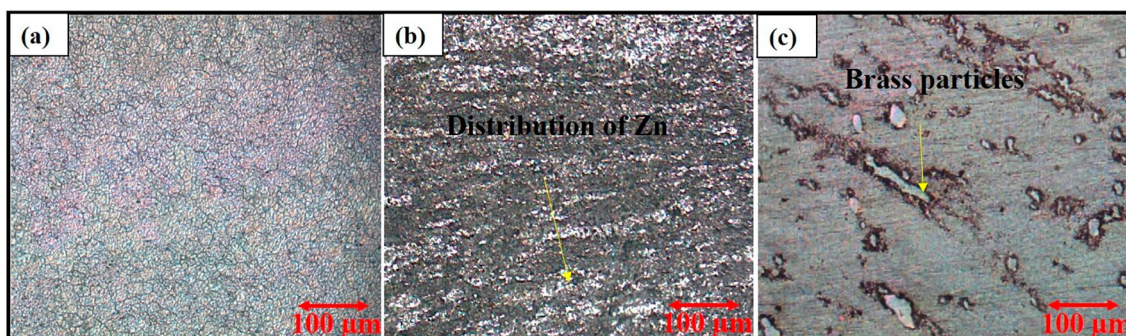


**Fig. 3** Microstructure of welds **a** without interlayer, **b** with Zn interlayer, and **c** with brass interlayer
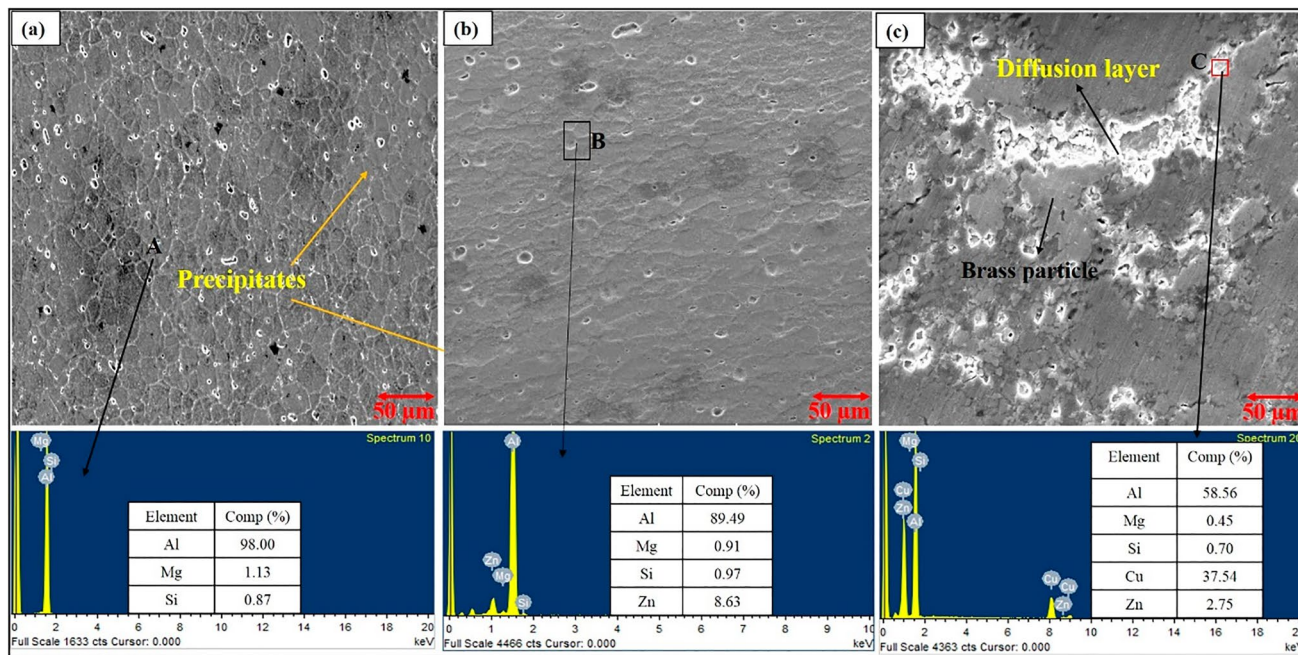
**Fig. 4** SEM images and EDAX of SZ of weld **a** without using interlayer, **b** with addition of Zn interlayer, and **c** with addition of brass interlayer
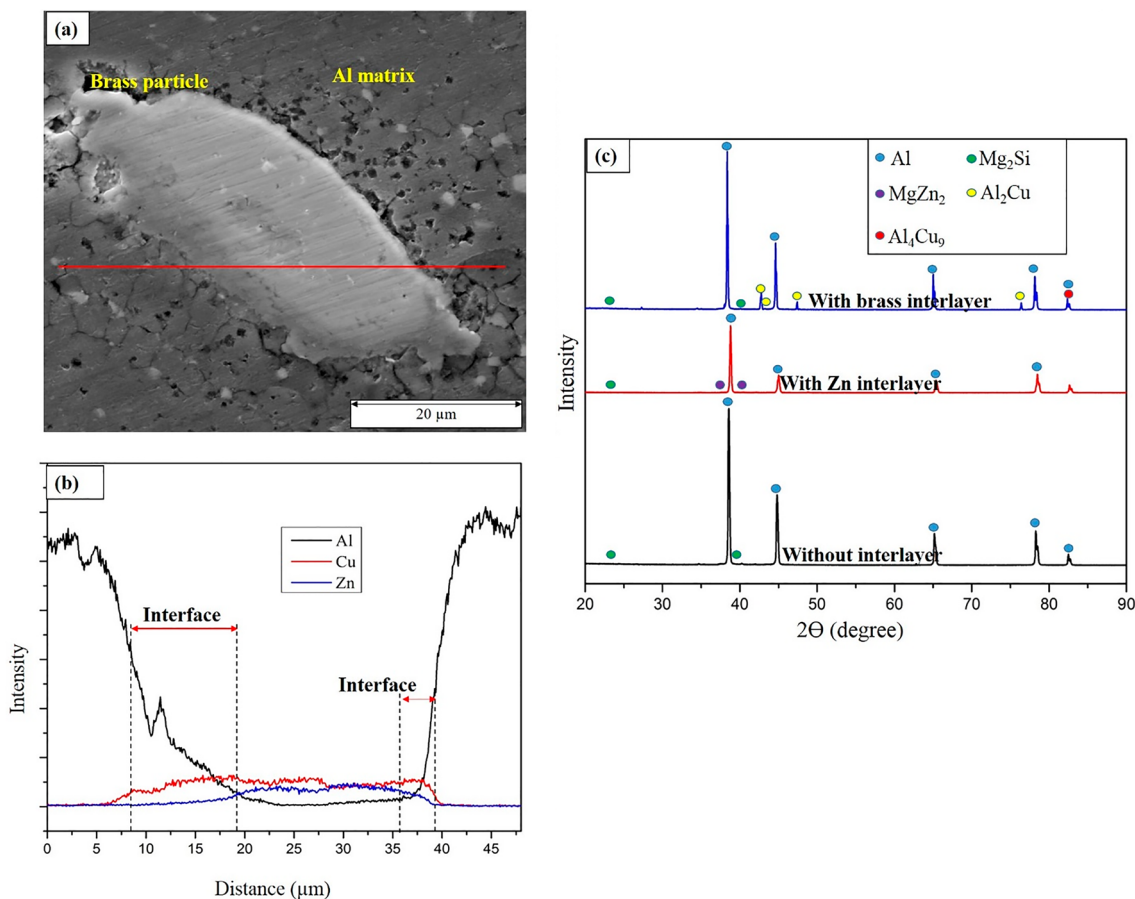


**Fig. 5** **a** SEM micrograph, corresponding- **b** EDS line scan curves and **c** XRD profile

The formation of IMCs was analyzed using EDAX analysis. Point A in Fig. 4a shows the presence of Mg and Si elements in Al matrix for weld without interlayer. In most 6 series Al alloys, the secondary phase particles are $Mg_2Si$, which is difficult to detect with SEM. Weld with Zn interlayer shows the existence of Zn in SZ, as shown in Fig. 4b. At the interface of brass and Al, the Al to Cu ratio was approximately 2, which is the same as $Al_2Cu$ intermetallics.

XRD analysis was performed to explore the confirmation of IMC formation. XRD profile of all weld joints is shown in Fig. 5c. More peaks of Al and formation of $Mg_2Si$ strengthening precipitates were observed for weld without interlayer. Earlier researchers also observed identical precipitates [13]. Weld with Zn interlayer did not form any strengthening IMCs attributed to Zn dissolving and diffusing in Al matrix. However, the presence of Zn element was observed for weld with Zn interlayer. $Al_2Cu$ and $Al_4Cu_9$ strengthening IMCs were observed for weld with brass interlayer. More $Al_2Cu$ intermetallics formed than $Al_4Cu_9$, indicating that $Al_2Cu$ is a dominating intermetallic distributed uniformly in SZ. Some researchers also observed the formation of Al-Cu intermetallics [14].

The grain structure of weld joints studied with EBSD analysis is presented in Fig. 6. Grain size, high angle grain boundaries (HABs), and low angle grain boundaries (LABs) fraction results are documented in Table 2. Figure 6d–f shows the HAB fractions for weld without interlayer, with Zn interlayer, and brass interlayer based on misorientation angle distribution. Grain refinement was observed in all weld joints due to dynamic recrystallization (DRX) and severe plastic deformation (SPD) during FSW.

A coarser grain structure was witnessed for weld without interlayer (Fig. 6a), and refined grains were observed for weld with interlayers (Fig. 6b and c). More grain refinement was found with the inclusion of brass interlayer, and a high percentage of HABs was attributed to brass, which led to further recrystallization [8]. The new grains began to grow after the recrystallization phase. Equation (1) relates the heating time during weld (*t*) and average grain size (*D*).

$$D - D_o = kt^n \tag{1}$$

At the start of the experiment, grain size ($D_o$), k is a constant. In most cases, the exponent n is lower than 0.5. However, the rise in temperature at FSW process parameters leads to lowering the solute atoms in the solid solution, so the n value may rise to 0.5. The interlayer's insertion and Zn's dissolution in Al matrix raise the number of impurity atoms, lowering n value [8]. Hence, better grain refinement occurred for the weld joint with interlayer than without interlayer.

Grain refinement and increase in high fraction of HABs were due to continuous DRX mechanisms and dynamic recovery (DRV). CDRX is an active DRX mechanism for Al alloys that can significantly impact grain structure evolution and result in finer grains [15]. DRV occurs during the hot deformation of metals such as Al alloys which possess high stacking fault energy. The addition of alloying elements to Al matrix has no considerable influence on stacking fault energy. Hence, the DRV mechanism is expected to prevail in Al alloys during hot deformation. During DRV, the increase in flow stress causes dislocations to multiply and interact during the early deformation stage. As subgrains emerge, the rate of recovery rises due to an increase in dislocation density, which causes the formation of LABs. At higher temperature deformation, dislocations are continually produced in the grains and subgrains to accommodate the strain incompatibility of adjacent grains and subgrains, thereby initiating CDRX. The subgrains grow and rotate in CDRX as dislocations are repeatedly absorbed into the subgrain boundaries, resulting in equiaxed recrystallized grains containing HABs [16]. Welds with interlayer have a larger volume fraction of HABs than welds without interlayer.

The hardness profile of the weld joints is shown in Fig. 7a. The average hardness of base metal is 105 Hv. Hardness decreased to 67 Hv after FSW for weld without using interlayer. Generally, $6 \times \times \times$ series Al alloys are precipitation-hardening alloys, and their mechanical properties depend on precipitation behavior rather than grain refinement. These precipitates may coarsen and dissolve at FSW process temperature [17]. The weld without interlayer showed low hardness in SZ due to the precipitates' dissolution and decreased dislocation densities. A marginal improvement of hardness in SZ (72 Hv) was perceived for weld with the addition of Zn interlayer due to solid solution formation with Al matrix. The highest hardness (85 Hv) for welding with brass interlayer was attributed to hard IMCs formation (Explained with SEM analysis). The distribution of detachable interlayer particles and the evolution of IMCs directly impact the hardness of interlayer welds. The lowest hardness in thermomechanically affected zone (TMAZ) and heat-affected zone (HAZ) for all weld joints was due to grain coarsening. The effect of partial deformation in TMAZ and the onset of thermal cycle in HAZ caused an increase in grain size in these zones.

Tensile results of weld joints are presented in Fig. 7b. Weld without using interlayer showed low strength (Fig. 7c), which could be attributed to the dissolution of precipitates and thermal softening. Weld with Zn interlayer showed a slight improvement in strength. Due to Zn melting and dissolving in Al matrix, a solid solution was formed with less significant improvement in mechanical properties. Dissolved Zn particles tried to reduce softening in SZ, but no intermetallics were formed. However, a slight improvement in strength (Fig. 7d) was observed, which was better than softened weld joint without using an interlayer attributed
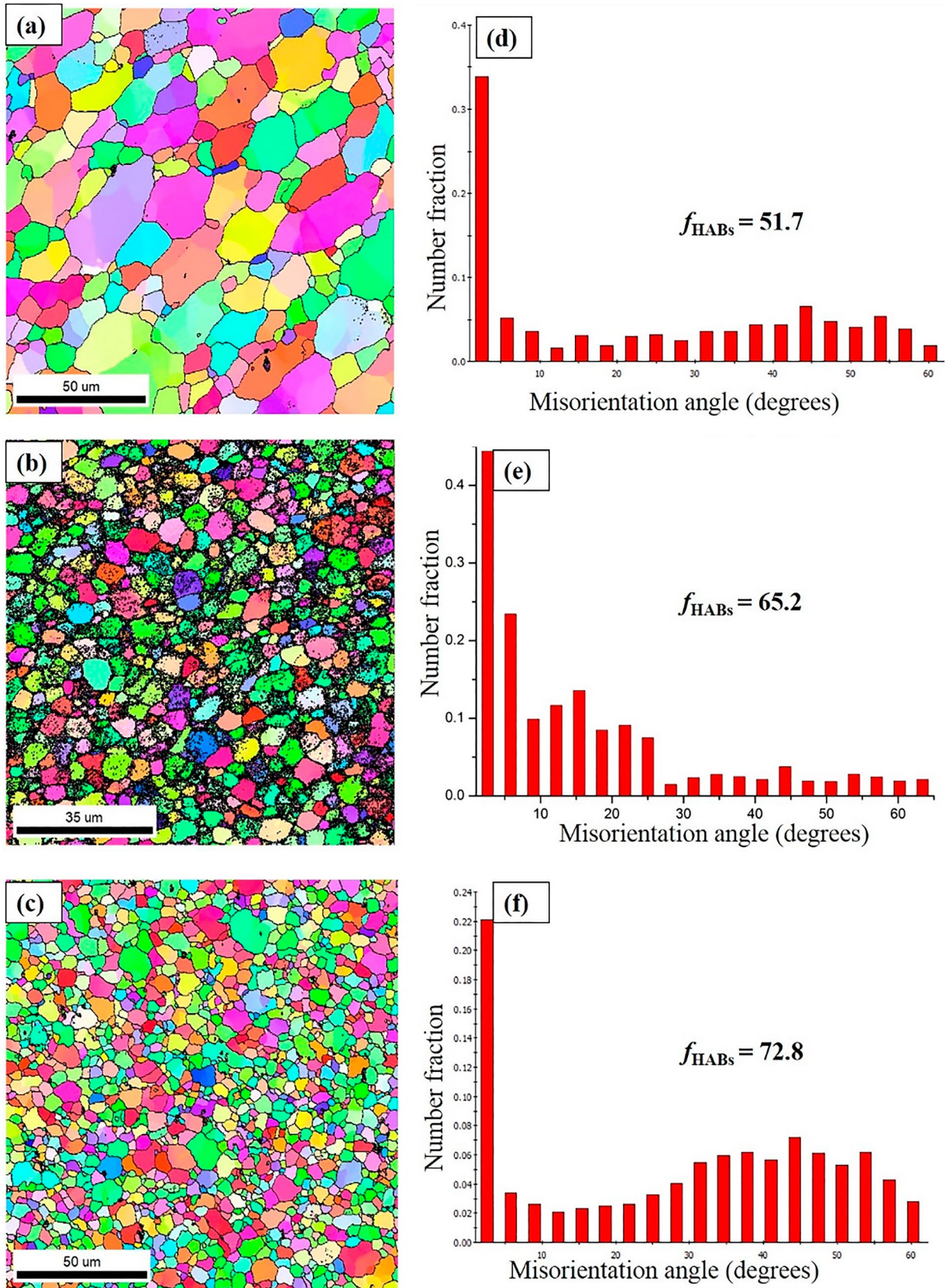
**Fig. 6** EBSD Microstructure and distribution of misorientation angle of welds **a** without using interlayer, **b** with addition of Zn interlayer, and **c** with addition of brass interlayer

**Table 2** EBSD results

| Samples | Grain size (µm) | Grain boundaries fractions (%) | |
| --- | --- | --- | --- |
| | | LABs (< 15°) | HABs (> 15°) |
| Base metal | 28.1 ± 3.1 | 72.9 | 27.1 |
| Without interlayer | 5.2 ± 0.6 | 48.3 | 51.7 |
| With Zn interlayer | 3.6 ± 0.4 | 34.8 | 65.2 |
| With brass interlayer | 2.3 ± 0.1 | 27.2 | 72.8 |

to filling the gaps or voids in SZ. Due to the production of strengthening IMCs (explained by SEM analysis), brass interlayer welds exhibited high strength (Fig. 7e), resulting in efficient metallurgical bonding at the interface. IMCs provided strong metallic interactions at the contact between brass and Al. Thus, this diffusion layer at the interface bound two materials (brass and Al) gradually, preventing significant metallurgical changes from compromising mechanical properties. Moreover, the lamellar dispersion of IMCs acted

as a barrier against the propagation of cracks. During the tensile test, when a load is applied, cracks prefer to move across regions with a high concentration of hard particles, while they deflect in areas with a low concentration of hard particles [14]. As a result of the aforementioned parameters, the weld strength with interlayer was enhanced.

Fracture features of tested tensile samples are shown in Fig. 8. All the fractures constituted varying sizes of dimples, indicating that a ductile shear fracture caused failure. Weld without interlayer shows large dimples, indicating ductile failure (Fig. 8a). The Zn interlayer weld exhibited a high density of small dimples, indicating ductile and brittle failure (Fig. 8b). Weld with brass showed small dimples and flat surfaces, indicating brittle failure (Fig. 8c) attributed to continuous dispersion of IMCs.

Figure 9a shows that initially all weld samples passed through a low-friction sliding mechanism before reaching the steady-state stage. The mean COF for weld without interlayer and with Zn interlayer is more, and it is less for weld with brass interlayer due to higher lubrication action of brass particles [18]. The lower COF of weld with brass
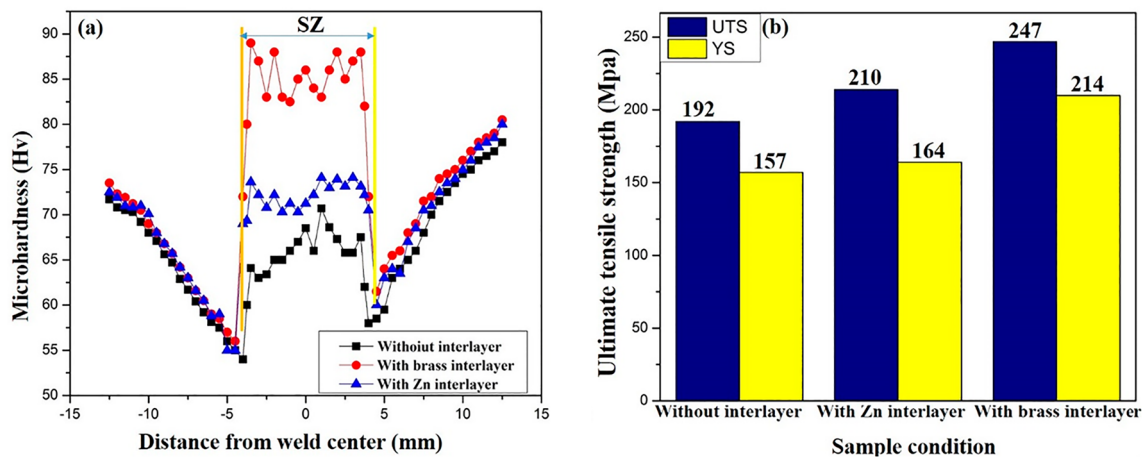


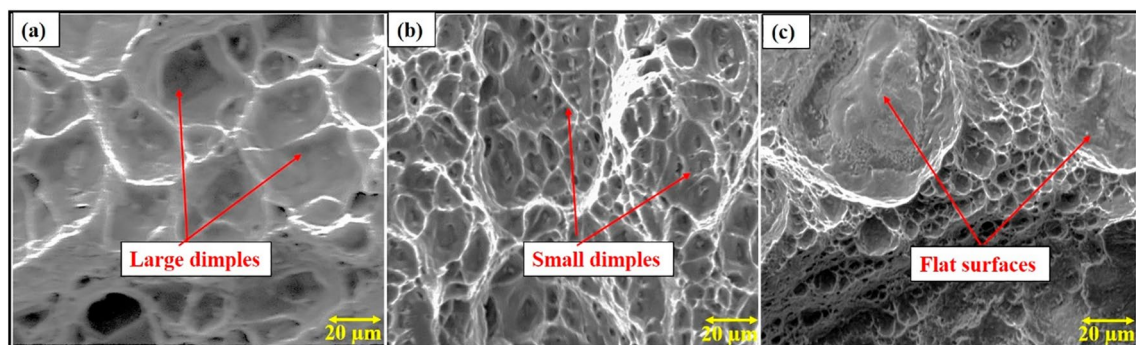**Fig. 7** **a** Microhardness profile of weld joints, **b** Tensile results of welds



**Fig. 8** Fracture morphology of welds **a** without interlayer, **b** with Zn interlayer, and **c** with brass interlayer
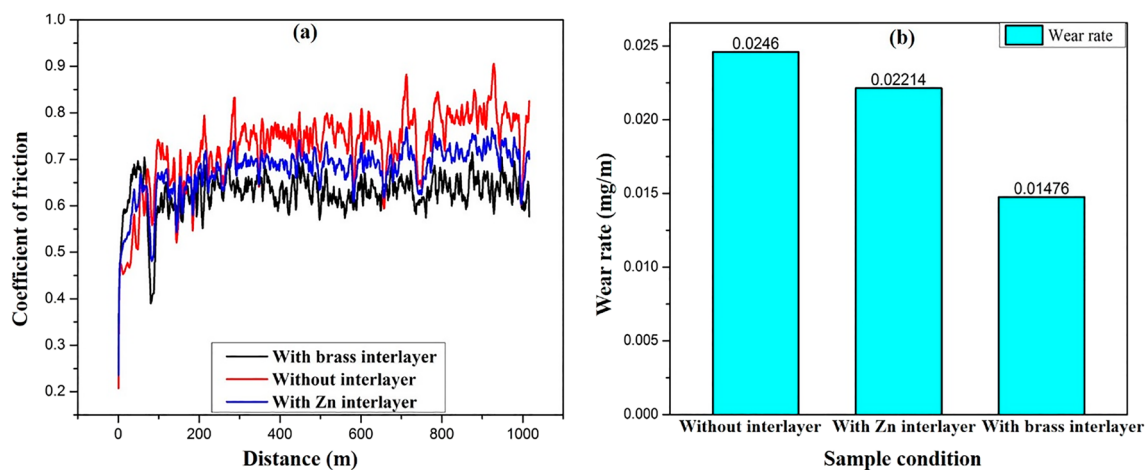
**Fig. 9** **a** Coefficient of friction variation, and **b** Wear rate of welds

interlayer is attributed to brass particle addition enhancing both hardness and bearing ability to decrease friction coefficient. Figure 9b shows the wear rate of weld joints with and without interlayers. The wear rate was more for weld without interlayers due to thermal softening and coarsening. The addition of Zn interlayer reduced softening, resulting in a reduction in wear rate. Minimum wear loss was observed for weld samples with brass interlayer due to more grain refinement and corresponding surface hardening [19]. Moreover, uniform dispersion of brass particles significantly impacts the wear rate of weld with brass interlayer.

Morphology of worn surfaces of welds with and without using interlayer after a sliding distance of 1000 m is displayed in Fig. 10. Each sample suffered various degrees of delamination, debris, cracks, and craters. Adhesive wear was signified by surface plastic deformation and the formation of delamination, which were more noticeable on the worn surface of a weld without an interlayer (Fig. 10a).

Also, scratches and grooves along the sliding direction on the worn surfaces of welds with Zn and brass interlayers (Fig. 10b and c) are signs of abrasive wear [10]. When comparing Figs. 10a, b, and c, it is clear that the weld surface with brass interlayer has low and shallow wear features. It is due to brass particles reinforcing effect, which enhances the material's wear resistance. Another indication of the weld with brass interlayer sample's superior wear resistance is the presence of more compact particles on its surface.

## 4 Conclusions

In the current investigation, interlayers of soft and hard materials have been used to reduce the softening, and the following conclusions emerged based on the study:
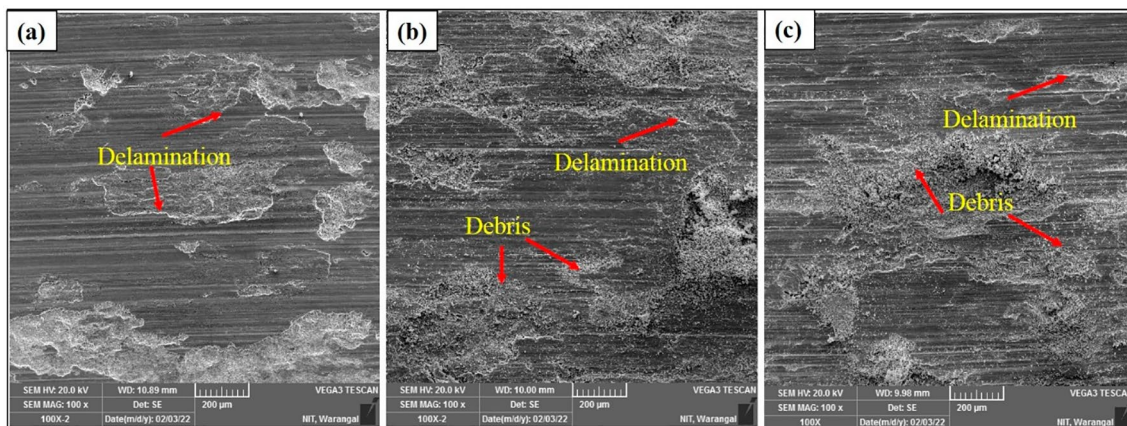


**Fig. 10** Worn surfaces of welds **a** without using interlayer, **b** with addition of Zn interlayer, and **c** with addition of brass interlayer

1. Weld with and without interlayer formed an equiaxed, fine grain structure. Better grain refinement was observed for weld using interlayer than without interlayer.

2. Zn particles melted, dissolved, and distributed uniformly in the SZ; no intermetallics were found for weld with Zn interlayer. Strengthening IMCs such as $Al_2Cu$ and $Al_4Cu_9$ were formed for weld with brass interlayer.

3. Marginal improvement in mechanical properties was observed for weld using Zn interlayer than without interlayer. The formation of IMCs was responsible for improved mechanical characteristics of the weld with brass interlayer.

4. Wear rate of the weld without using interlayer was higher, and it was minimized for weld with interlayer. Minimum wear rate for weld with brass interlayer was due to better grain refinement and corresponding surface hardening.

## References

1. Satyanarayana M V N V, and Kumar A, *Proc Instit Mech Eng Part L: J Mater: Design Appl* (2021). https://doi.org/10.1177/14644207211005790
2. Mishra R S, and Ma Z Y, *Friction Stir Welding Process* **50** (2005) 1–78.
3. Wang T, Zou Y, and Matsuda K, *Mater Design* **90** (2016) 13–21.
4. Gharavi F, Amin K, and Yunus R, *Integr Med Res* **4** (2015) 314.
5. Chandran R, Kumar S, Santhanam V. Submerged Friction Stir Welding of 6061-T6 Aluminium Alloy under Different Water Heads. 21.
6. Yi J, Wang G, Li S, Liu Z W, and Gong Y, *Trans Nonferrous Met Soc China* **29** (2019) 2035.
7. Khojastehnezhad V M, and Pourasl H H, *Trans Nonferrous Met Soc China* **28** (2018) 415.
8. Mokabberi S R, Movahedi M, and Kokabi A H, *Mater Sci Eng A* **727** (2018) 1.
9. Wilson A, Lenin A, Periyasamy N, and George L, *Mat Res* **19** (2016) 817–823.
10. Alishavandi M, RazmjooKhollari M A, Ebadi M, Alishavandi S, and Kokabi A H, *J Alloys Compd* **83** (2020) 2. https://doi.org/10.1016/j.jallcom.2020.153964
11. Zohoor M, Givi M K B, and Salami P, *Mater Design* **39** (2012) 358–365.
12. Esmaeili A, Givi M K B, and Rajani H R Z, *Mater Sci Eng: A* **528** (2011) 7093.
13. Malopheyev S, Vysotskiy I, Kulitskiy V, Mironov S, and Kaibyshev R, *Mater Sci Eng A* **662** (2016) 136.
14. Esmaeili A, Rajani H R Z, Sharbati M, Givi M B, and Shamanian M, *Intermetallics* **19** (2011) 1711–1719.
15. Yu P, Wu C S, and Shi L, *Acta Mater* **20** (2021) 7. https://doi.org/10.1016/j.actamat.2021.116692
16. Mcnelley T R, Swaminathan S, and Su J Q, *Recrystall Mech During Friction Stir Welding/Process Aluminum Alloys* **58** (2008) 349–354.
17. Satyanarayana M V N V, Adepu K, and Chauhan K, *Metals Mater Int* **27** (2021) 3563.
18. Palanivel R, Dinaharan I, Laubscher R F, and Davim J P, *JMADE* **106** (2016) 195.
19. Mehta K M, and Badheka V J, *Wear* **426–427** (2019) 975.